13th International Symposium on Turbulence and Shear Flow Phenomena (TSFP13)
Montreal, Canada, June 25–28, 2024

COMPARATIVE ANALYSIS OF THE MIXING CHARACTERISTICS OF SLOT- AND DUCT TWIN-JET IMPINGEMENTS: A SENSITIZED-RANS STUDY

Steffen Gröninger, Maximilian Bopp, Suad Jakirlić
Department of Fluid Mechanics and Aerodynamics
Technical University of Darmstadt
Peter-Grünberg-Straße 10, 64287 Darmstadt
groeninger@sla.tu-darmstadt, jakirlic@sla.tu-darmstadt.de

ABSTRACT

This study focuses on the numerical analysis of two perpendicular impinging jet configurations consisting of two in-parallel exiting streams — twin jets — with different concentrations, with particular emphasis on their mixing characteristics. While the nozzle design of the so-called Double Square Impinging Jet (DSIJ) resembles two three-dimensional ducts arranged side by side, the second flow configuration considered, referred to as Double-Slot Geometry (DSG), represents a modification of the DSIJ case by enforcing the condition of flow homogeneity in the spanwise direction. Impinging jets are known for their high complexity, characterized by, among other phenomena, strong streamline curvature caused by sudden changes in flow direction, which requires careful consideration in numerical modeling. In this study, RANS-based approaches (Reynolds-Averaged Navier-Stokes) are used to analyze turbulent redistribution and mixing processes using Reynolds Stress Model (RSM) formulations. To evaluate their accuracy, the performance of a conventional RSM is compared with that of an Improved Instability-Sensitive RSM (IISRSM), highlighting the latter's capability to resolve turbulence fluctuations to a reasonable extent. The study evaluates key parameters such as velocity and Reynolds stress fields and mixing behavior. The work provides insight into the formation of mixing layers and species transport within these geometries. The superiority of the IISRSM over the conventional RSM is demonstrated, especially in correctly capturing the turbulence quantities that play a critical role in assessing mixing efficiency.

INTRODUCTION

The high complexity involved in the numerical analysis of impinging jets is a well-known problem that requires careful consideration. This complexity is due to factors such as strong streamline curvature, alternating flow deceleration and acceleration correlated with the sign change of the velocity and pressure gradients, representing the main sources of extensive turbulence generation. When using RANS-based approaches, extensive modeling is required to adequately capture the underlying redistribution processes among the Reynolds stress components. However, for single planar impinging jets, an appropriate Reynolds Stress Model (RSM) class can resolve the flow with reasonable accuracy. Based on this knowledge, this study investigates a more complex geometry known as the Double Square Impinging Jet (DSIJ). The DSIJ is an impingement configuration consisting of a twin-jet configuration emanating from two three-dimensional square ducts and impinging perpendicularly side-by-side on the same plate positioned at a certain distance from the DSIJ nozzle exit. The addition of another duct to the configuration not only increases the complexity of the flow, but also allows for intense mixing processes to occur between the duct outlets and the impingement plate, which are not well understood despite their common occurrence in industrial applications. The double-slot geometry (DSG), which is simulated additionally, represents a simplification of the DSIJ towards a two-dimensional configuration with respect to the mean flow field. In this study, different modeling approaches are used to simulate these flows, comparing a baseline RSM solution with that of an (Improved) Instability-Sensitive RSM (IISRSM). This comparison can be used to demonstrate the improvements of the IISRSM model over the baseline RSM model due to its eddy-resolving capability. All solutions are referenced to a well-resolved Large Eddy Simulation (LES) performed as part of this project.

COMPUTATIONAL METHODOLOGY

For a thorough comparison of model capabilities, it is necessary to obtain reference data against which to evaluate. For this purpose, either a direct numerical simulation (DNS) or experimental data are obvious choices, since they do not rely on models. When using a DNS, convergence is necessary to ensure correct data sets, but is difficult to achieve at the high spatial and temporal resolutions required for such complex flow configurations. For experimental data, on the other hand, there is always a mismatch between experimental and numerical data sets, due to differences in e.g. the geometric model or the resolution of the hardware versus the order of different algorithms. Therefore, it is useful to compute an LES with sufficient resolution to be used as a benchmark dataset and computed on the exact same geometric domain. For this LES, the Wall-Adaptive Local Eddy-viscosity (WALE) model (Nicoud & Ducros (1999)) is used for the subfilter scales due to its advantageous near-wall behavior compared to the classical Smagorinsky model (see Wegt *et al.* (2022) for a corresponding analysis). All simulations in this study are performed using the RANS-based equations of motion under the assumption of incompressible flow:

$$\frac{D\overline{U_i}}{Dt} = -\frac{\partial \overline{p}}{\partial x_i} + \frac{\partial}{\partial x_j}\left(\nu \frac{\partial \overline{U_i}}{\partial x_j} - \overline{u_i'u_j'}\right). \tag{1}$$

In the case of baseline RSM, $\overline{U_i}$ represents a time-averaged velocity field, while the IISRSM scheme allows the instantaneous character of the underlying velocity field to be captured. For the closure of the stress tensor $\overline{u_i'u_j'}$, an RSM formulation is used in the form:

$$\frac{D\overline{u_i'u_j'}}{Dt} = P_{ij} + \Phi_{ij} - \varepsilon_{ij}^h + 0.5D_{ij}^{\nu} + D_{ij}^{u'} \quad (2)$$

where the terms on the right-hand side denote the production rate P_{ij}, the redistribution process Φ_{ij}, the viscous dissipation ε_{ij}^h $(= \varepsilon_{ij} - 0.5\nu\partial^2\overline{u_i'u_j'}/(\partial x_l \partial x_l))$, and various diffusion terms $D_{ij}^{\nu}, D_{ij}^{u'}$. The production rate P_{ij} and the viscous diffusion D_{ij}^{ν} can be treated exactly, while the other terms must be modeled. For the conventional RSM model, the formulation proposed by (Jakirlić & Hanjalić (2002)) is used. This model has been further extended with the aim of sensitizing it to capture turbulent fluctuations (Jakirlić & Maduta (2015)), in accordance with the scale-adaptive simulation (SAS) method proposed by Menter & Egorov (2010). Consequently, the scale-resolving IISRSM includes an additional production term (P_{SAS}) in the transport equation, which determines the specific dissipation rate $\omega^h = \varepsilon^h/k$ with $\varepsilon^h = 0.5\varepsilon_{ii}^h$ and $k = 0.5\ \overline{u_i u_i}$.

$$\frac{D\omega_{\mathrm{SAS}}^h}{Dt} = \frac{D\omega^h}{Dt} + P_{\mathrm{SAS}}, \quad P_{\mathrm{SAS}} = f\left(\nabla^2\overline{U_i}\right) \quad (3)$$

The functional dependence of the additional production P_{SAS} on the second derivative of the velocity field allows the model to be adapted to the scales present in the unresolved residual motion. This interaction is handled by increasing the transport of ω^h for the resolved spectrum by interacting with the underlying grid resolution, allowing the development of resolved turbulent fluctuations. It is important to note that the choice of the trigger length scale, which determines whether to resolve or model within the SAS approach, is not the von Kármán length scale, as originally proposed by Menter & Egorov (2010) in their $k-\omega-SST-SAS$ model, but is derived from a term related only to the second velocity derivative, as given in the integral length scale equation of Rotta (1972). This increases sensitivity and allows for even coarser grids due to the grid-independence of the model formulation itself. The detailed model specification is given in Jakirlić & Maduta (2015) and different flow geometries are calculated for its validation, see among others Joksimović & Jakirlić (2023) and Bopp *et al.* (2024).

The species concentration is modeled by means of a scalar transport equation as follows:

$$\frac{\partial\overline{C}}{\partial t} + \frac{\partial}{\partial x_i}\left(\overline{U_i C}\right) = \frac{\partial}{\partial x_i}\left(\frac{\nu}{Sc}\frac{\partial\overline{C}}{\partial x_i} - \overline{u_i'c'}\right) \quad (4)$$

To account for the unclosed turbulent scalar flux, this study focuses on two common modeling approaches representing the $\overline{u_i'c'}$ dependence on the concentration gradient. The first is the Simple Gradient Diffusion Hypothesis (SGDH) (Daly & Harlow (1970)):

$$\left(-\overline{u_i'c'}\right)_{\mathrm{SGDH}} = \Gamma_t\frac{\partial\overline{C}}{\partial x_i}, \qquad \text{with} \qquad \Gamma_t = \frac{\nu_t}{Sc_t} \quad (5)$$

and the second approach is the Generalized Gradient Diffusion Hypothesis (GGDH) (Daly & Harlow (1970); $\tau = k/\varepsilon^h$):

$$\left(-\overline{u_i'c'}\right)_{\mathrm{GGDH}} = D_{ij}\frac{\partial\overline{C}}{\partial x_j} \qquad \text{with} \qquad D_{ij} = k\tau C_C\frac{\overline{u_i'u_j'}}{k} \quad (6)$$

The main between these two approaches lies in the formulation of the coefficient function that multiplies the concentration gradient, with the GGDH model allowing for a dependence on the anisotropic Reynolds stress tensor, which accounts for the turbulence anisotropy involved in the redistribution process.

The model equations are implemented in the finite-volume-based numerical code OpenFOAM with second-order accuracy in space and time, which is used for all simulations.

COMPUTATIONAL DOMAIN

Two different flow configurations are considered in this study. The first flow configuration is the perpendicular impingement of two jets emerging from a double duct nozzle with a square cross-section on a flat wall (Double-Square Impinging Jet - DSIJ), as shown in Fig. 1 (upper). The second configuration is similar to the first, except that the ducts are not rectangular but infinite along the z-axis, resembling two plane channels. This is achieved by using a spanwise extent of three times the duct width D to allow physically correct turbulent motion, and the front plane is arranged symmetrically to the back plane (Double-Slot Geometry - DSG), as shown in Fig. 1 (lower), with periodic flow conditions applied to it. The flow in the ducts and channels is under fully-developed conditions. All simulations are performed with an inflow Reynolds number of $\mathrm{Re_b} = \mathrm{U_b D}/\nu = 10000$, where $\mathrm{U_b}$ represents the inlet velocity and the molecular Schmidt number is $Sc = 0.7184$.

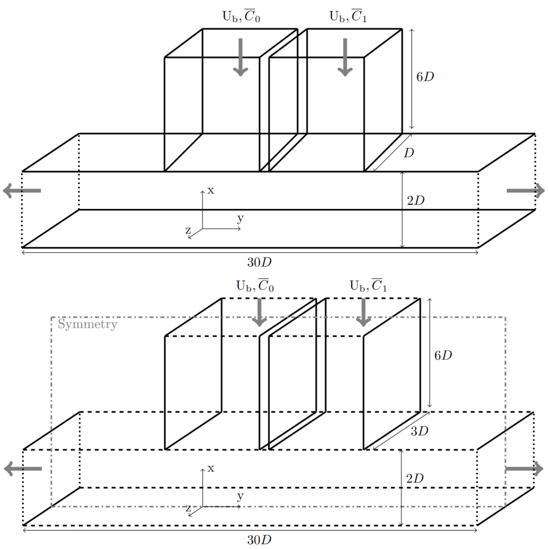

Figure 1. Schematic of the double-square impinging jet (DSIJ, upper) and double-slot geometry (DSG, lower) domains

Both geometries can be divided into three parts: the precursor, the inlet, and the impingement or outlet region. The inlet consists of the two ducts/channels. The impingement or outlet region is the area below the nozzle outlet towards the bottom plate. This is where the impingement process takes place. The flow within the inlet ducts/channels is computationally realized by a separate precursor simulation for each duct/channel. The statistically independent, fully developed duct/channel flow is generated by applying periodic conditions to the inflow/outflow planes of the precursor. The resulting instantaneous flow fields are then mapped to the corresponding main inlets of the vertical channel. To provide an overview of the spatial resolution, the mesh is divided into the number of cells in the precursor, inlet, and impingement regions.

For the DSIJ configuration, only the precursor and inlet can be specified in Cartesian coordinates, and the impingement area resolution refers to the total number of cells. Precursor and inlet of the DSIJ domain have the same number of cells in both cross-sectional directions y and z with the same aspect ratio. In Table 1 all dimensions are listed for the DSIJ. For the DSG on the other hand, the impingement and exit regions are not round, and therefore the cells in the impingement region are also given in Cartesian coordinates. In this case, the number of grid cells in the spanwise and crosswise directions z and y is not equal, as shown in Table 2.

Model	$N_{i,\mathrm{precursor}}$	$N_{i,\mathrm{inlet}}$	N_{total}
LES	$x = 102$	240	42.0 mio
	$y,z = 90$	90	
IISRSM	$x = 25$	40	1.4 mio
	$y,z = 30$	30	
RSM	$x = 1$	50	1.3 mio
	$y,z = 25$	25	

Table 1. DSIJ: Number of grid cells used for the different turbulence models; for precursors and inlet ducts the number of cells in all coordinate directions is given

Model	$N_{i,\mathrm{pre}}$	$N_{i,\mathrm{inlet}}$	$N_{i,\mathrm{impingement}}$	N_{total}
LES	$x = 100$	180	200	32.6 mio
	$y = 140$	140	1236	
	$z = 100$	100	100	
IISRSM	$x = 50$	90	110	4.3 mio
	$y = 70$	70	608	
	$z = 50$	50	50	
RSM	$x = 100$	180	200	0.4 mio
	$y = 140$	140	1236	
	$z = 1$	1	1	

Table 2. DSG: Number of grid cells used for the different turbulence models

To investigate scalar species transport and mixing processes, one inflow duct contains a passive, numerically fully dissolved species ($C_1 = 1$), while the other inflow duct contains no further species ($C_0 = 0$). Furthermore, all boundary conditions for the velocity and Reynolds stress fields on all walls are set to no slip for both the DSIJ and DSG configurations, which is consistent with asymptotically correct behavior of all flow variables and periodic conditions on the spanwise planes for the DSG configuration. A zero-gradient boundary condition for the species C is applied to the boundary walls and all outlets. There are no temperature variations.

RESULTS AND DISCUSSION

Fig. 2 provides a first impression of the flow structure by showing the Q-criterion colored by the non-dimensionalized instantaneous species field for both considered twin-jet impinging configurations, clearly illustrating the eddy-resolving inherence of the present IISRSM, applied in conjunction with the GGDH scalar-flux modeling scheme.

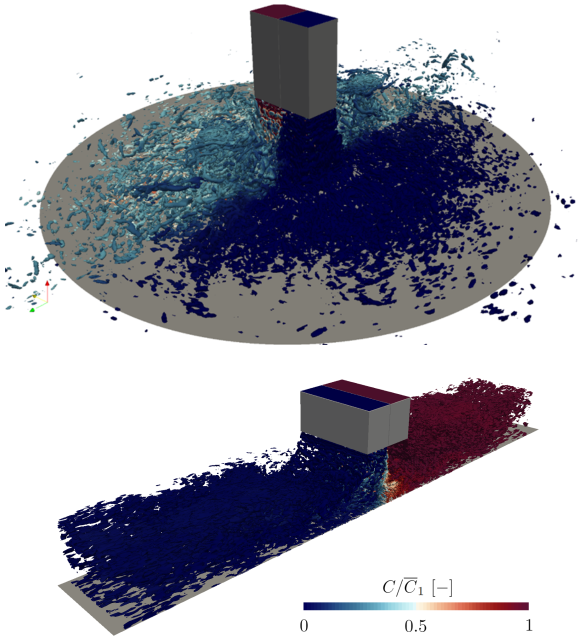

Figure 2. Flow visualization by Q-criterion, colored by the non-dimensionalized instantaneous concentration field for the DSIJ (upper) and DSG (lower) configurations obtained by the scale-resolving IISRSM

Precursor LES for inlet duct and channel

In this subsection, the quality assessment of the LES with respect to the generation of the fluctuating inflow in both twin-impingement configurations is provided. For this purpose, the precursor is compared with external DNS data and two different quality criteria are used to show, that the resolution is sufficiently high. Fig. 3 displays multiple subplots illustrating the profiles of the velocity, turbulent kinetic energy and normal Reynolds stress components. Each variable profile on the left is related to the DSG configuration, with the DNS database at a comparable Reynolds number of $Re_b = 13750$ from Iwamoto (2002). The variable profiles on the right side refer to the DSIJ configuration compared to the DNS of Vinuesa *et al.* (2018), which is based on a fully enclosed duct at $Re_b = 11386$ with a friction-based Reynolds number of $Re_\tau = 356$ in the central duct plane. In the first row of Fig. 3 the normalized streamwise velocity u^+ is shown for both configurations, closely following the DNS data in each characteristic region of the channel/duct cross section. Similarly high prediction quality is obtained for the turbulent kinetic energy (TKE) k profiles shown in the second row of Fig. 3 and the normal Reynolds stress components shown in the last row. To further elaborate the mesh quality, the ratio between the modeled and the total TKE k_{SGS}/k and between the filter size and the Kolmogorov length Δ/η are evaluated and compared with the values given by Pope (2000). Table 3 gives an overview of the standard maximum values from the literature and the corresponding values obtained in this study.

Double-Square Impinging Jet

For the DSIJ configuration, Figure 4 shows the time-averaged velocity field obtained by the conventional RANS-RSM and the instantaneous velocity fields obtained by both scale-resolving models, IISRSM and LES, in the central vertical midplane. The velocity fields show a highly complex

Domain	k_{SGS}/k	Δ/η
Pope (2000)	≤ 0.2	$10\ldots12$
DSIJ	0.068	11.41
DSG	0.13	10.48

Table 3. Overview of the quality criteria for the LES grid resolution given by Pope (2000) and their maximum values for the two flow configurations

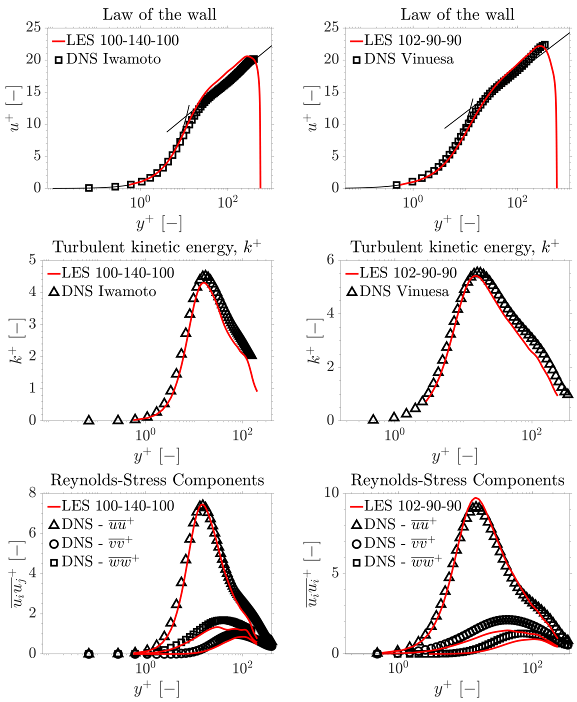

Figure 3. Velocity, turbulent kinetic energy and Reynolds stress profiles obtained by the present LES of the DSG (left) and the DSIJ (right) configurations compared to the relevant DNS data

flow structure with a strong flow bifurcation after impingement. This process is associated with an alternation of the velocity gradient from a negative one, implying a sudden deceleration due to the impingement, to the intense acceleration immediately afterward, accompanied by a strong streamline curvature. The IISRSM-related results are obtained under the conditions of a significantly coarser grid resolution compared to the LES, as listed in Table 1 (the same is valid for the conventional RSM).

The flow field shown in Fig. 4 is characterized by different phenomena typical for the flow impingement. Due to the confinement by a three-dimensional wall-bounded duct geometry, the outlet streams are directed strictly downward until reaching the impact point at the bottom plate; the flow deceleration following the strong pressure increase immediately at the plate, characterized by flow stagnation, forces the flow into a sharp 90-degree inclination to a wall jet that spreads radially along the plate. Therefore, the wall jet is limited to the lower part of the outflow region. Comparing the IISRSM and LES-related results, the capability to resolve a variety of length scales of turbulent structures is evident. The overall flow field looks similar for all cases, but the structures in between the ducts, especially visible in the IISRSM and LES-related flow fields, indicate that their mixing onset takes place already in

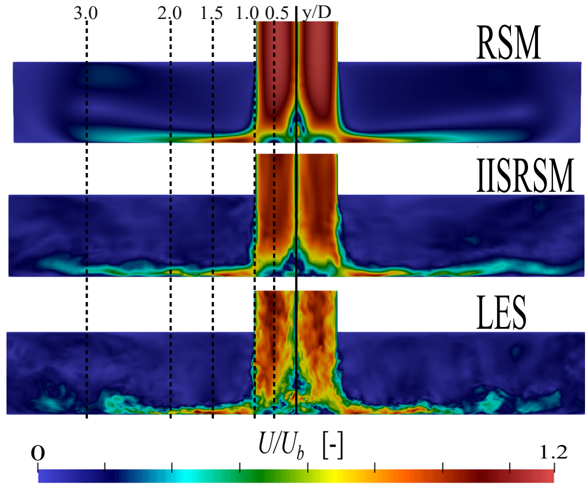

Figure 4. DSIJ: Velocity field obtained by the baseline RSM and the scale-resolving IISRSM and LES models

this area. An enhanced interaction of both jets takes place in the lower part of the outflow region, coinciding with the impingement center. The flow pattern in the area coinciding with the twin-jet impact shows entrained regions with significantly reduced flow momentum, as indicated by the distinctly weakened intensity of the velocity field. The flow pattern in the area coinciding with the twin-jet impact shows a confined region with significantly reduced flow momentum, as indicated by the significantly weakened intensity of the velocity field., Fig. 4. To evaluate this mixing region in more detail, the fields of the TKE are provided in Fig. 5. For each of the sub-figures, it is possible to identify the boundaries of the downward-facing flow that represent the areas of increased flow straining turbulent kinetic energy enhancement, although there is a noticeable difference in magnitude. Both RSM-based models underestimate the intensity of the TKE, suggesting that a higher percentage of resolved length scales leads to a better estimation of the mixing process.

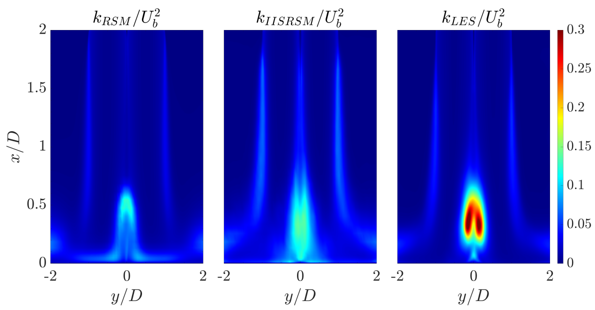

Figure 5. DSIJ: Turbulent kinetic energy field obtained by the baseline RSM and the scale-resolving IISRSM and LES models

Apart from the mixing region, another interesting phenomenon of this configuration can be seen within the horizontal outflow channel. As shown in Fig. 4, strong streamline curvature is an important flow characteristic, and a large amount of turbulence intensity is distributed from the downward-facing normal Reynolds stress component $\overline{uu}$ into the outward-facing, plate-parallel component $\overline{vv}$. In Fig. 6, the profiles of both components are plotted at several positions within the outflow region, including the immediate impingement region ($y/D = 0.5$ and 1.0) and the three locations crossing the wall jet region. The upper figure shows the RST component $\overline{uu}$

profiles for each turbulence model. It can be seen that the RSM based models tend to overestimate the RST component intensity in the impingement region. The overall higher estimate associated with the baseline RSM is a known result of excessive turbulence production due to streamline curvature (see e.g. Bopp *et al.* (2024)). The IISRSM related turbulence level estimation, although much smaller, indicates the need for even better spatial resolution. Progressing outward, all profiles show the turbulence intensity decreasing and the mismatch decreasing. The lower plots in Fig. 6 show the profiles of the outward-facing turbulent stress component $\overline{vv}$. Comparing the IISRSM with the RSM, the eddy resolution capability seems to increase the accuracy. The total component intensity increases as the wall jet develops. The near-wall peaks are correctly reproduced, as well as the intensity maxima that coincide with the flow shearing at the wall jet boundary (locations $y/D = 1.5 - 3.0$). In summary, the plots show that the magnitude of the downward-directed stress component decreases as the outward-directed stress component increases.

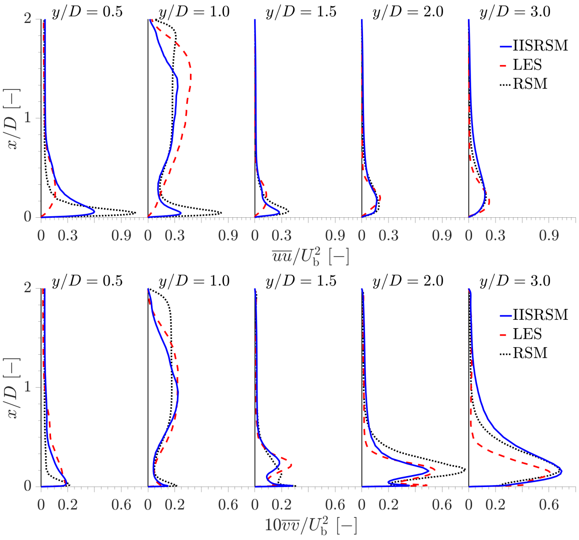

Figure 6. DSIJ: Profile development of the Reynolds stress components of the two dominant directions in the impingement process

Double-Slot Geometry

The basic structure of the flow field of the DSG domain shown in Fig. 7 is strikingly different from that of the DSIJ case. The lateral propagation of the jets exiting the double slot nozzle starts much closer to the nozzle outlet and exhibits a curvature with a milder gradient than the DSIJ configuration in Fig. 4. Comparing the performance of the turbulence models, the improved predictive capabilities of the scale-resolving approaches are even more apparent. The baseline RSM is capable to return the time averaged flow field adequately, but the associated flow field seems to show a weak mixing activity between the two outflowing jets. Looking at the IISRSM and the LES results, the transport processes that take place are clearly indicated by the coherent eddies in the middle of the geometry, and therefore the DSG is characterized by a mixing region between the channels, even if the wall jets do not collide at the bottom wall. The triangular shape of this region is a consequence of a plane configuration geometry with two outlets. The earlier start of lateral jet propagation, closer to the nozzle exit, is responsible for strong flow shearing at the outer sharp edge of the nozzle. The flow shedding at the sharp nozzle edge induces an increased proportion of turbulent energy in the upper layer of the outflow channel. The enhancement of the flow straining can be clearly recognized in the vortical structure intensification at the jet borders in Fig. 7, but also at the TKE profiles shown in Fig. 8.

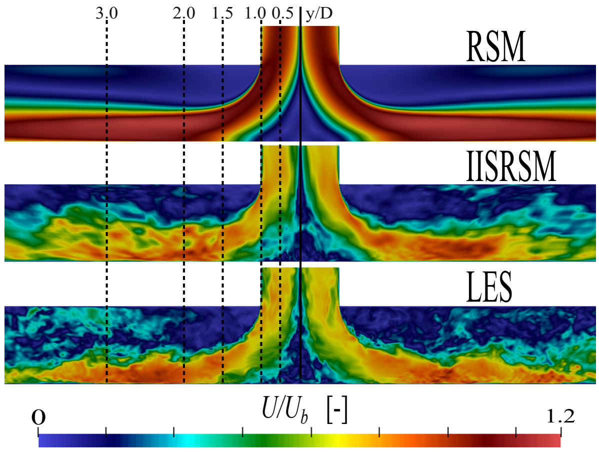

Figure 7. DSG: Velocity field obtained by the baseline RSM and the scale-resolving IISRSM and LES models

Fig. 8 shows the TKE field in the impingement region. The turbulence models qualitatively predict the highest intensity in the center of the channels and a reasonable increase in TKE coinciding with the jet edges. Comparing the IISRSM and LES results, the TKE distribution in terms of intensity is very similar, with a slight difference in the region of mutual jet interaction. For the inner triangular zone, the scale-resolving models determine a much higher turbulent intensity level, which differs strongly from the low turbulence level that characterizes the baseline RSM. This is clearly visible in the profiles of the Reynolds stress components shown in Fig. 9.

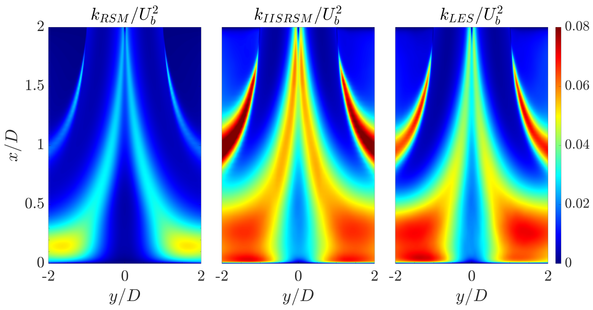

Figure 8. DSG: Turbulent kinetic energy field obtained by the baseline RSM and the scale-resolving IISRSM and LES models

The TKE field shown in Fig. 8 is characterized by the two maxima coinciding with the jet boundaries, which represent the areas of highest velocity gradients. This is clearly seen in the profiles of the downward ($\overline{uu}$) and outward ($\overline{vv}$) Reynolds stress components shown in Fig. 9. The profile shapes are generally analogous to those of the DSIJ, but there are important differences. Starting with the upper row of Fig. 9, the shape at $y/D = 1.5$, $y/D = 2.0$ and $y/D = 3.0$ develops the characteristic double peak. The lower peak is the result of the transition from downward to outward flow direction, but the upper peak corresponds to the increased turbulent production

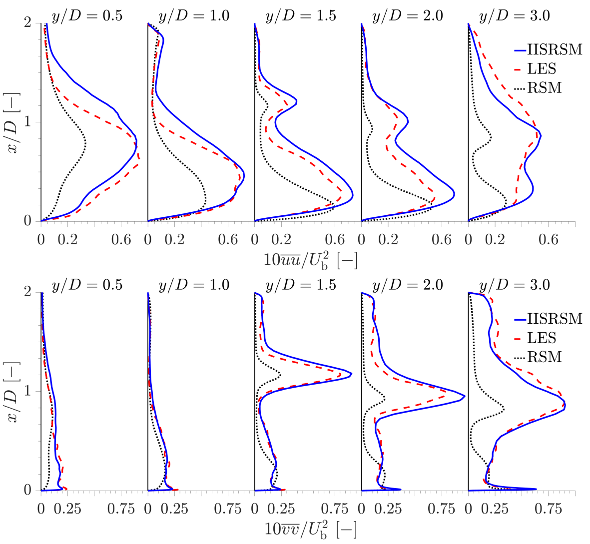

Figure 9. DSG: Profile development of the Reynolds stress components of the two dominant directions in the impingement process

resulting from the flow passing the sharp edge of the nozzle. The outward RST component $\overline{vv}$ is shown in the lower row and is characterized by the systematic increase of the near-wall peak and the longer persistent maximum corresponding to the wall jet development. Compared to the DSIJ-related profiles in Fig. 6, the turbulence intensities of the DSG already reach maximum values at the location $y/D = 1.5$ whose vertical position, i.e. the distance to the bottom wall, decreases as the flow approaches the outlet planes. This observation correlates with the velocity field in Fig. 7, where the global flow direction partially remains downward even in the outer region of the flow domain.

Fig. 10 shows the instantaneous passive scalar field of both DSIJ and DSG configurations obtained by the IISRSM, visualizing the mixing process. It is obvious that the enhanced scalar transport occurs across the interface separating the two jets, although the main difference in terms of mixing intensity comes from the geometric properties of the two configurations. While for the DSIJ domain all the passive scalar C_1 entering the outflow channel is concentrated in the close proximity of the bottom impingement wall with very weak interaction with the remaining part of the outflow domain, in the DSG configurations the mixing process is much more intense, occupying the larger part of the outflow channel cross section. Furthermore, the mixing activity of the DSIJ is characterized by a stronger scalar gradient between the channels, whereas for the DSG the gradient is milder and the mixing region is much wider. Furthermore, the generation of large coherent eddies in both fields indicates that the main transport is induced by convection resulting from a high inflow momentum of the jets, reducing the influence of different diffusion models; a similar result is obtained with the GGDH model.

CONCLUSIONS

The present work illustrates an intensive computational study of in-parallel flowing differently structured jets in two different flow configurations, a true three-dimensional Double-Square Impinging Jet and a nominally two-dimensional Double-Slot Jet. The aim of the study is to gain a deeper understanding of the mixing processes during the impingement

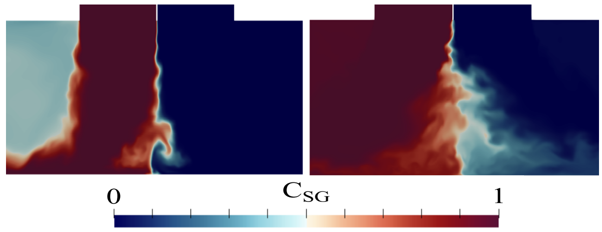

Figure 10. Field of the passive scalar ratio, calculated with the SGDH approach (Eq. 5), for the DSIJ configuration (left) and the DSG configuration (right)

of a twin jet, which will help to develop eddy-resolving modeling approaches and test them in complex flow scenarios. For the present study, the IISRSM model is shown to provide a thorough simulation without the need for increased resource input as in the case of a fine-resolution LES, which is the main objective of this research area.

Acknowledgements. The financial support of the German Research Foundation (DFG) in the framework of the Collaborative Research Center/Transregio 150 (SFB-TRR 150, Project Number 237267381) is gratefully acknowledged. The authors furthermore would like to thank for the computing time granted on the Lichtenberg HPC at TU Darmstadt.

REFERENCES

Bopp, M., Wegt, S., Krüger, L., Secchi, F., Frohnapfel, B. & Jakirlić, S. 2024 Heat flux modeling in impinging flows using a Reynolds stress turbulence closure within RANS and Sensitized-RANS frameworks. *Int. J. Heat and Fluid Flow* **105**, 109264.

Daly, B.J. & Harlow, F.H. 1970 Transport equations in turbulence. *Physics of Fluids* **13** (11), 2634–2649.

Iwamoto, K. 2002 Database of fully developed channel flow. *THTLAB Internal Report* .

Jakirlić, S. & Hanjalić, K. 2002 A new approach to modelling near-wall turbulence energy and stress dissipation. *Journal of Fluid Mechanics* **459**, 139–166.

Jakirlić, S. & Maduta, R. 2015 Extending the bounds of 'steady' RANS closures: Toward an instability-sensitive reynolds stress model. *Int. J. Heat and Fluid Flow* **51**, 175–194.

Joksimović, I. & Jakirlić, S. 2023 Eddy-resolving Reynolds-stress modelling of thermal mixing in cross-stream type T-junction configurations. *Applied Thermal Engineering* **235**, 121390.

Menter, F. R. & Egorov, Y. 2010 The scale-adaptive simulation method for unsteady turbulent flow predictions. part 1: Theory and model description. *Flow, Turbulence and Combustion* **85** (1), 113–138.

Nicoud, F. & Ducros, F. 1999 Subgrid-scale stress modelling based on the square of the velocity gradient tensor. *Flow, Turbulence and Combustion* **62** (3), 183–200.

Pope, S.B. 2000 *Turbulent Flows*. Cambridge University Press, ISBN: 9780511840531.

Rotta, J. 1972 *Turbulente Strömungen*. Wiesbaden: Vieweg+Teubner Verlag, ISBN: 978-3-322-91207-7.

Vinuesa, R., Schlatter, P. & Nagib, H. M. 2018 Secondary flow in turbulent ducts with increasing aspect ratio. *Phys. Rev. Fluids* **3**, 054606.

Wegt, S., Maduta, R., Kissing, J., Hussong, J. & Jakirlić, S. 2022 LES-based vortical flow characterization in a 90°-turned pipe bend. *Computers & Fluids* **240**, 105418.